JETIR.ORG ISSN: 2349-5162 | ESTD Year : 2014 | Monthly Issue
JOURNAL OF EMERGING TECHNOLOGIES AND INNOVATIVE RESEARCH (JETIR)
An International Scholarly Open Access, Peer-reviewed, Refereed Journal

Multi-Instrument observations of Thunderstorms, Lightning Activity and Precipitation Microphysics over Kadapa, Southern India

V. Mallikarjuna Reddy[1,2], and K.Krishna Reddy[3]*

[1]Research Scholar & [2]Post-graduate Teacher, [3]Professor
[1]Department of Physics, Rayalaseema University, Kurnool, Andhra Pradesh, India
[2]A.P.Model School and Junior College, Punganur, Andhra Pradesh, India
[3]Yogi Vemana University, Kapada, Andhra Pradesh, India
* Correspondence Author

Abstract: *This study investigates thunderstorm characteristics, lightning activity, and precipitation microphysics over Kadapa, southern India, using integrated multi-instrument observations. Ground-based lightning sensors, Micro Rain Radar (MRR), PARSIVEL disdrometer, automatic weather station, and GPS radiosonde measurements were analysed. The long-term observations (2013–2022) indicate an average of 47 thunderstorms annually, with enhanced lightning activity during the pre-monsoon and post-monsoon seasons. Comparison of MRR and PARSIVEL measurements revealed strong agreement in radar reflectivity (R^2 = 0.9665) and rainfall rate (R^2 = 0.9552). Ground-based lightning observations also showed strong correspondence with TRMM-LIS measurements (R^2 = 0.903Overall, the findings demonstrate the value of integrated atmospheric observations for understanding thunderstorm evolution, lightning characteristics, and precipitation processes over southern India.*

Index Terms: Thunderstorms; Lightning activity; Micro Rain Radar; PARSIVEL disdrometer; Radiosonde thermodynamics; CAPE; Precipitation microphysics.

I. INTRODUCTION

Thunderstorms are complex atmospheric systems characterized by intense convection, lightning discharges and precipitation. Their development is influenced by atmospheric instability, moisture availability, vertical wind shear, boundary-layer processes and seasonal monsoon circulation. Over the Indian subcontinent, these factors produce considerable spatial and temporal variability in thunderstorm activity, particularly during pre-monsoon and monsoon transition periods [1]–[4].

Thunderstorm electrification is primarily associated with interactions among ice crystals, graupel and supercooled water droplets within mixed-phase clouds. These processes contribute to charge separation and lightning generation (Saunders). Lightning frequency and temporal variations therefore provide useful information about convective activity, although they cannot independently describe storm intensity or precipitation characteristics. Satellite observations, including the Tropical Rainfall Measuring Mission Lightning Imaging Sensor (TRMM-LIS), have demonstrated the value of lightning measurements for investigating regional convective variability (Christian et al.) [5], [6] [5], [6], [27], [30].

Precipitation microphysics provides complementary information about storm development. Micro Rain Radar (MRR) observations characterize the vertical structure of precipitation through radar reflectivity and Doppler fall velocity, while PARSIVEL disdrometers measure hydrometeor diameter and fall velocity near the surface. These measurements enable the investigation of raindrop-size distributions, rainfall characteristics and melting-layer signatures (Peters et al.; Löffler-Mang et al.). Furthermore, radiosonde-derived parameters, including Convective Available Potential Energy (CAPE), Convective Inhibition (CIN), TTI and SWEAT indices, help characterize atmospheric conditions favourable for convection. However, thunderstorm development depends not only on instability but also on moisture availability, lifting mechanisms and vertical wind shear (Doswell and Rasmussen) [7]–[15].

The interior region of Kadapa, Andhra Pradesh, provides an important setting for investigating thunderstorm variability over southern India. However, understanding regional convective activity requires the combined examination of lightning characteristics, precipitation microphysics and atmospheric thermodynamic conditions rather than relying on individual observational parameters [1]–[3].

The present study uses observations from the Semi-Arid-Zonal Atmospheric Research Centre (SARC), Yogi Vemana University, Kadapa, integrating long-term lightning records (2013–2022), event-based lightning telemetry, MRR, PARSIVEL disdrometer, GPS radiosonde, automatic weather station and satellite observations. The objectives are to characterize seasonal and temporal lightning variability, investigate precipitation structure and raindrop-size distributions, compare ground-based lightning measurements with TRMM-LIS observations, evaluate MRR–PARSIVEL measurement consistency, and examine the thermodynamic environment associated with convective development [16]–[18].

The principal contribution is the integration of electrical, thermodynamic and precipitation-microphysical observations within a unified framework for characterizing thunderstorms over Kadapa. This approach provides complementary insights into regional convective activity and establishes an observational basis for distinguishing thunderstorm, non-thunderstorm, hailstorm, convective and stratiform precipitation regimes [11], [12], [15].

II. SITE DESCRIPTION AND INSTRUMENTATION

2.1 Study location

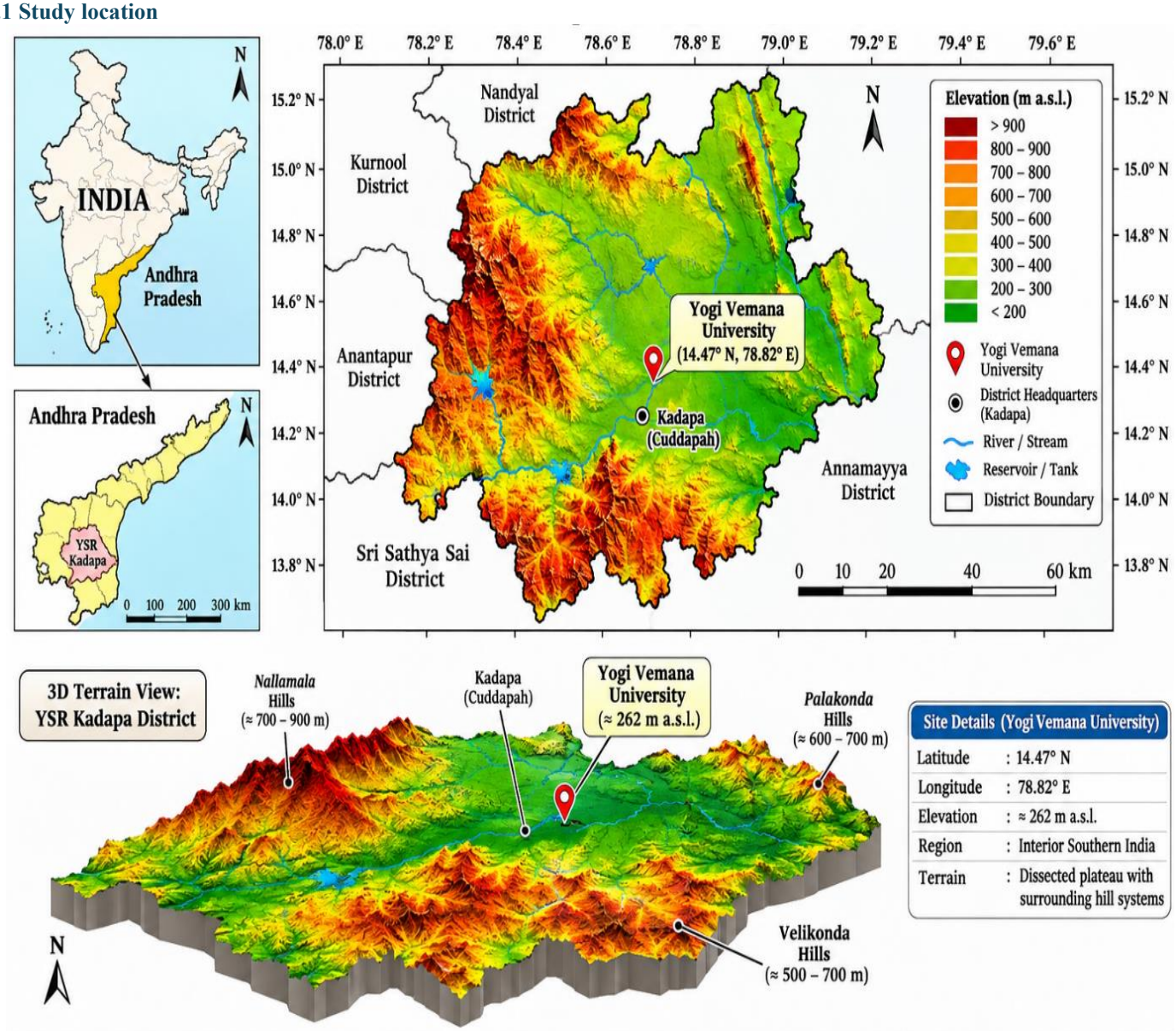

Figure 1. Geographical location and three-dimensional topographic representation of YSR Kadapa district, Andhra Pradesh, India, showing the location of the Yogi Vemana University (YVU) observational site at approximately 14.47° N, 78.82° E. The elevation-coloured terrain highlights the regional relief, dissected plateau surfaces, and surrounding hill systems, illustrating the physiographic setting of the study area. The inset maps show the location of Andhra Pradesh within India and the position of YSR Kadapa district within the state.

Kadapa (also known as Cuddapah), Andhra Pradesh, is located at approximately 14.47°N, 78.82°E, as specified in the study brief. The site is situated in the interior of southern India, within a region of dissected plateau terrain and surrounding hill systems. Figure 1 illustrates the geographical location and topographic setting of the Yogi Vemana University (YVU) observational site in YSR Kadapa district, Andhra Pradesh, India. The geographical and three-dimensional topographic representation of YSR Kadapa Kadapa (also known as Cuddapah) district provides the physiographic context of the atmospheric observational site established at Yogi Vemana University (14.47° N, 78.82° E), Andhra Pradesh, India. The study region is situated in the interior part of southern India and is characterized by dissected plateau terrain, variations in surface elevation, and surrounding hill systems. The elevation-coloured terrain and three-dimensional visualization demonstrate the spatial heterogeneity of the regional landscape. These topographic characteristics provide an important geographical framework for investigating atmospheric boundary-layer processes, local circulation patterns, moisture transport, and convective precipitation development. In particular, the interaction between regional terrain and atmospheric conditions may contribute to the spatial and temporal variability of thunderstorms and associated precipitation over the study region. Therefore, the topographic setting is an important consideration when interpreting the lightning, radar reflectivity, rain-rate, and thermodynamic observations collected at the YVU atmospheric research facility.

2.2. Observational Systems



Figure 2. Overview of the observational facilities, and instrumentation at Semi-Arid-Zonal Atmospheric Research Centre (SARC), Yogi Vemana University, Kadapa, Andhra Pradesh, India. (a) Field observation facility showing the lightning sensor (LS), automatic weather station (AWS), Monsoon Weather Station, PARSIVEL disdrometer (PSD), and Micro Rain Radar (MRR); (b) SARC supercomputer facility supported by the Indian Space Research Organisation (ISRO), showing the computing infrastructure and server system; (c) GPS radiosonde launch for upper-air atmospheric observations; (d) ISRO-AWS and mini-boundary-layer mast.

The observation site, Yogi Vemana University Campus (14^0 28' N 78^0 42' E, 150 m above mean sea level), is about 15 km from Kadapa city in the southern part of India [as shown in *figure 1.*] . Micro Rain Radar (MRR) collocated with PARSIVEL disdrotmer, lightning sensor, GPS Sonde and AWS are utilized to separated precipitating cloud type and cloud fractions into Hailstorm, thunderstorm, non-thuenderstorm, convective and stratiform . MRR is capable of providing vertical structure of Precipitation and vertical structure of RSD profiles. MRR is a low cost vertical profiling radar used to determine the enhanced radar reflectivity at zero degree isotherm (Bright Band). In the present work heavy precipitation events associated with maximum rainrate value greater than 100 mm/h are only considered. The RSD of such heavy precipitation events observed in SW (8568 minutes) and NE (7020 minutes) monsoon seasons of the years 2013 and 2022 are utilized.

Figure 2 presents an overview of the integrated atmospheric observation and research infrastructure established at the Semi-Arid-Zonal Atmospheric Research Centre (SARC), Yogi Vemana University, Kadapa, Andhra Pradesh. The facility comprises complementary ground-based and upper-air observational instruments, supported by computational infrastructure, to investigate atmospheric conditions, precipitation characteristics, lightning activity and thunderstorm development over the semi-arid region of southern India [24], [25].

Panel (a) illustrates the main field observation facility and its ground-based instrumentation. The lightning sensor (LS) is used to monitor lightning activity, while the Automatic Weather Station (AWS) records near-surface meteorological parameters. The Monsoon Weather Station provides additional meteorological observations. The PARSIVEL disdrometer (PSD) measures raindrop size and fall velocity distributions, enabling the investigation of precipitation microphysical characteristics and estimation of rainfall parameters. The Micro Rain Radar (MRR) provides vertical profiles of precipitation-related parameters, including radar reflectivity, rain rate and fall velocity. The simultaneous operation of these instruments facilitates the comparison of surface precipitation measurements with vertically resolved radar observations and lightning activity [7]–[9], [15], [24].

Table 1: Technical Specifications of the Micro Rain Radar (MRR)

Parameter	Specification
Radar frequency	24.1 GHz
Wavelength	1.25 cm
Transmit power	50 mW
Modulation	FM-CW
Beam direction	Vertical
Beam width (2-way, 6 dB)	2°
Antenna	Offset parabola
Radome	No
Range resolution	100 m
Lowest analysed range	300 m
Number of range gates	30
Time resolution	1 min
Spectral velocity resolution	0.191 m/s
Nyquist velocity range	0–12.3 m/s
Number of power spectra (1 min)	≈10^3
Minimum detectable radar reflectivity at 1000 m	−2 dBZ

Table 2: PARSIVEL (LASER) disdrometer specifications:

Transmitter Wavelength	780 nm
Measurement Area	48.6 cm^2
Radar Reflectivity	-9 to 99 dBZ
Rain Rate	0.01 to
Particle size	0.25 to 25 mm
Particle velocity	0.1 to 20 m/s
Rainfall accumulation	0.01 to 9999 mm
Sampling time	1 min

Table 2.3: *Specifications of the Automatic Weather Station.*

Variable	Required sensors	Resolution	Range	Accuracy
Barometric pressure	Included in console	0.1 mb	540–1100 mb	1 mb
Inside humidity	Included in console	1%	1–100%	3% RH
Outside humidity	ISS or Temp/Hum station	1%	1–100%	3% RH
Daily & storm rainfall	Rain collector	0.2 mm	0.2–999.8 mm	1 tip / 4%
Inside temperature	Included in console	0.1 °C	0 to +60 °C	0.5 °C
Outside temperature	ISS or Temp/Hum station	0.1 °C	−40 to +65 °C	0.5 °C
Time	Included in console	1 min	24 hours	8 sec/month
Date	Included in console	1 day	Month/day	8 sec/month
Wind direction	Anemometer	1°	0–360°	3°
Wind speed	Anemometer	0.4 m/s	1–80 m/s	1 m/s

Panel (b) shows the SARC supercomputer facility supported by the Indian Space Research Organisation (ISRO). The computing infrastructure, including server racks and monitoring systems, provides computational support for processing, analysing, modelling and storing atmospheric observational data. Such facilities are important for handling the large datasets generated by the different instruments and conducting integrated analyses of thunderstorm and precipitation events [24], [25].

Panel (c) depicts a GPS radiosonde launch conducted for upper-air atmospheric observations. The radiosonde, carried by a weather balloon, measures vertical profiles of atmospheric pressure, temperature, relative humidity and wind speed and direction. These measurements are used to derive thermodynamic parameters, including Convective Available Potential Energy (CAPE), Convective Inhibition (CIN) and other atmospheric stability indices. Such parameters help evaluate the thermodynamic environment favourable for convective cloud development and thunderstorm initiation [19]–[23], [24].

Panel (d) presents the ISRO Automatic Weather Station and the mini-boundary-layer mast. These installations provide complementary meteorological observations near the surface and within the lower atmospheric boundary layer. Their measurements help characterize local atmospheric conditions and investigate variations in meteorological parameters that may influence boundary-layer evolution and convective development [24], [25].

The observational infrastructure at SARC provides a multi-instrument framework for investigating thunderstorms through the combined analysis of lightning, surface meteorology, precipitation microphysics, vertical radar structure and upper-air thermodynamic conditions. The integration of the lightning sensor, AWS, PSD, MRR and radiosonde observations enables the examination of relationships between atmospheric instability, precipitation formation, rainfall intensity and electrical activity. The computational facility further supports the processing and interpretation of these diverse datasets. Consequently, the SARC observational network provides an important experimental foundation for understanding the initiation, evolution and precipitation characteristics of thunderstorms over the Kadapa region [7]–[15], [24].

Table 4. Observational systems identified in the supplied research material and metadata needed for reproducibility.

System	Role in the analysis	Required metadata
Lightning detector	Electrical event counts, flash/stroke rates and event timing	Sensor type, detection efficiency, location, time resolution, event/flash definition, polarity and duration algorithm
Micro Rain Radar	Vertical precipitation structure and Doppler spectra	MRR model, frequency, range gates, vertical resolution, temporal averaging, spectral processing and calibration
PARSIVEL disdrometer	Surface drop-size distribution and precipitation spectra	Model, sampling area, bin limits, velocity/diameter corrections and quality-control thresholds
Radiosonde	Pressure, temperature, humidity and derived instability indices	Manufacturer/model, launch times, pressure/height profiles, humidity correction, parcel method and sounding files
AWS / Boudary Layer mast	Surface temperature, humidity, pressure, wind and rainfall	Sensor models, heights, calibration, sampling cadence and data completeness
Satellite products	Cloud shield, cloud-top and regional convective context	Satellite/platform, product name, channel, spatial/temporal resolution and retrieval version

III. DATA USED IN THE STUDY

The present study uses a multi-instrument observational dataset collected at the Semi-Arid-Zonal Atmospheric Research Centre (SARC), Yogi Vemana University, Kadapa, Andhra Pradesh, India (14.47° N, 78.82° E). The dataset combines long-term lightning observations, event-based lightning telemetry, precipitation radar measurements, Micro Rain Radar (MRR) observations, disdrometer measurements and upper-air radiosonde profiles. These complementary observations are used to examine thunderstorm occurrence, lightning activity, precipitation structure and the thermodynamic environment associated with convective development over the semi-arid region of southern India [16]–[18], [24].

The principal datasets and their scientific applications are summarized in Table 5:.

Dataset	Parameters considered	Purpose in the study
Long-term thunderstorm records (2013–2022)	Annual thunderstorm frequency	Establishing the local thunderstorm climatology
Lightning telemetry	Stroke counts, occurrence time and duration	Examining lightning activity and its temporal evolution
Weather radar	Reflectivity and Doppler velocity	Investigating precipitation structure and convective development
Micro Rain Radar	Vertical reflectivity, fall velocity, rain rate and liquid water content	Characterizing vertical precipitation structure
PARSIVEL disdrometer	Drop diameter, fall velocity and rainfall rate	Examining surface precipitation and drop-size distributions
GPS radiosonde	Pressure, temperature, humidity and wind profiles	Deriving thermodynamic instability indices
AWS	Surface Pressure, temperature, humidity, Wind speed and direction	Local climate
Satellite observations	TRMM/GPM Satellite observations: Spatial distribution of lightning and convective activity	Providing regional context for selected events

The long-term lightning dataset was used to characterize thunderstorm occurrence and lightning activity over Kadapa during 2013–2022. The source material reports an average of 47 thunderstorms per year during this period. This climatological information provides the background against which individual thunderstorm events and their associated electrical activity are examined. The lightning observations include the number of detected strokes, event duration and temporal variations in lightning activity. The lightning-monitoring system comprises multiple sensors, allowing the recorded stroke activity from different sensors to be examined comparatively. The supplied observational material also includes annual and monthly lightning distributions and thunderstorm-case statistics. The reported annual thunderstorm frequency is treated here as a value from the SARC source dataset; it should not be interpreted as an independently verified district-wide climatological estimate [1]–[3], [16], [17].

The long-term climatological component covers 2013–2022, while the event-based lightning analysis focuses on selected observations from October 2022. The MRR dataset includes comparative precipitation structures for hailstorm, thunderstorm and non-thunderstorm conditions, together with selected comparisons between MRR and PARSIVEL measurements. Radiosonde observations provide the thermodynamic context for interpreting the observed convective activity.

IV. DATA QUALITY CONTROL AND VALIDATION

To ensure the reliability of the observational dataset, appropriate quality-control procedures should be applied before conducting integrated analyses. These procedures include [24], [25]:

1. Calibration verification: Check the calibration status and manufacturer specifications of all instruments.
2. Range checks: Identify observations outside physically reasonable measurement limits.
3. Temporal consistency: Examine missing records, irregular sampling intervals and unrealistic sudden changes.
4. Inter-instrument comparison: Compare simultaneous PSD and MRR measurements of reflectivity and rainfall rate.
5. Lightning data verification: Examine the consistency of stroke records from the multiple lightning sensors and identify possible false detections.
6. Radiosonde quality assessment: Check vertical continuity and physically plausible variations in pressure, temperature, and humidity profiles.

4.1 Micro Rain Radar and PARSIVEL disdrometer observations

Micro Rain Radar (MRR) and PARSIVEL disdrometer observations form an important component of the precipitation dataset. The vertically pointing MRR provides time-dependent vertical profiles of precipitation parameters, including radar reflectivity, Doppler fall velocity, rain rate and liquid water content. Its Doppler spectra can also be used to retrieve raindrop size distribution (DSD) and associated microphysical parameters. The PARSIVEL optical disdrometer, installed near the surface, measures the size and fall velocity of individual precipitation particles, enabling the estimation of ground-level raindrop size distributions and rainfall characteristics. Simultaneous measurements from these instruments facilitate comparisons between surface-based precipitation measurements and vertically resolved radar observations. Such combined observations have been widely employed to investigate precipitation microphysics and evaluate the consistency of radar-derived rainfall parameters against disdrometer measurements.

Figure 3 illustrates the vertical and temporal evolution of rainfall observed on 9 July 2022 using MRR and disdrometer measurements. The initial period (approximately 04:30–05:50 IST) exhibits strong radar reflectivity, intense rainfall, and larger raindrop diameters (up to approximately 5–6 mm), indicating vigorous convective activity. A second, weaker precipitation episode occurs around 06:20–06:50 IST, followed by relatively light rainfall between 07:10 and 08:05 IST. The corresponding reduction in radar reflectivity, rainfall rate, and raindrop diameter indicates the gradual weakening of precipitation. Overall, the combined observations demonstrate the evolution of multiple precipitation phases and highlight the complementary capabilities of MRR and disdrometer measurements in characterising rainfall structure and microphysical properties [7]–[15]

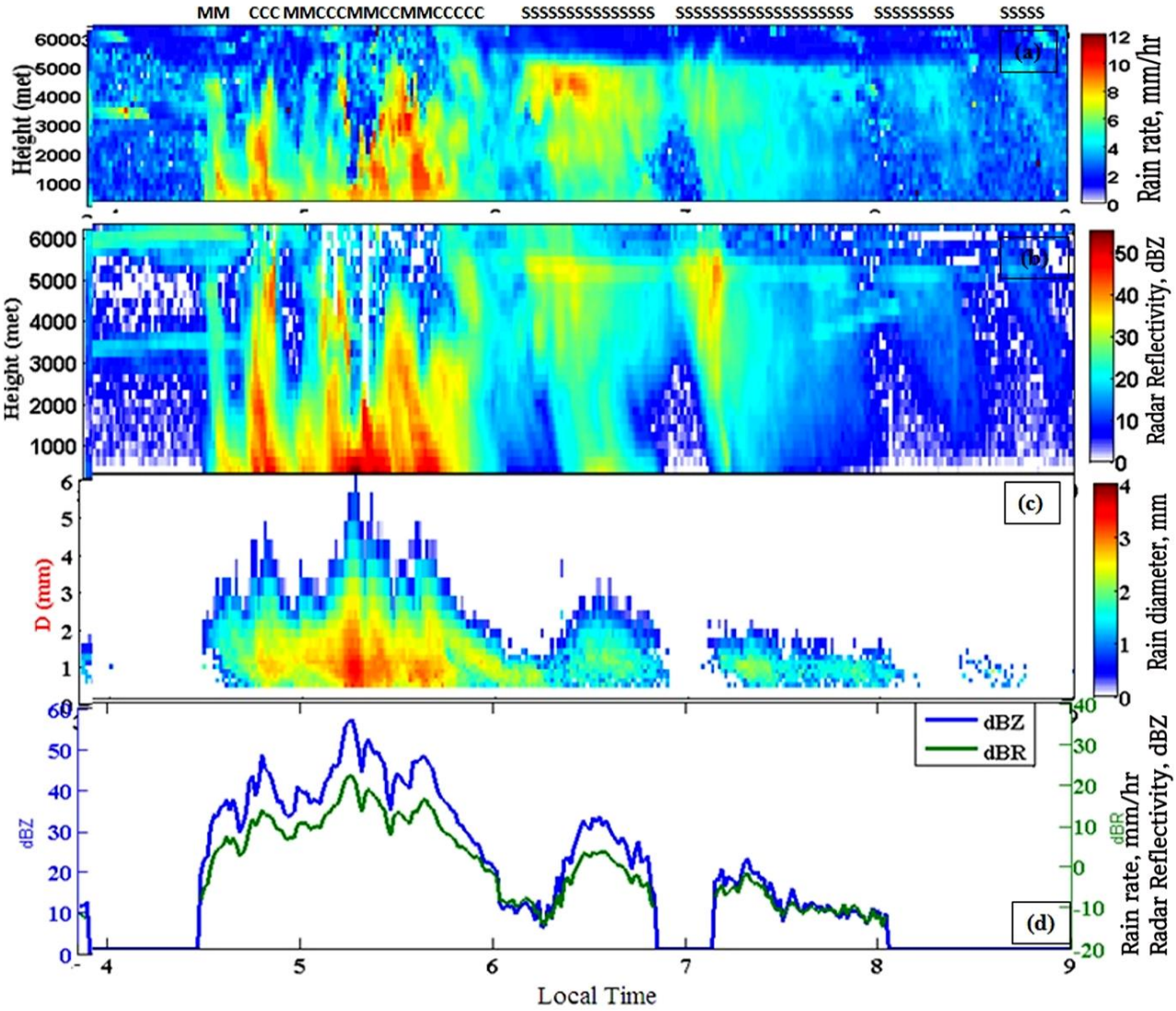

Figure 3. Time–height evolution of rainfall and radar characteristics observed over Kadapa on 9 July 2022. (a) Time–height cross-section of 1-min rainfall rate (mm h^{-1}) derived from the vertically pointing Micro Rain Radar (MRR). (b) Corresponding vertical distribution of radar reflectivity (dBZ) measured by the MRR. (c) One-minute disdrometer-derived raindrop size distribution, expressed in terms of raindrop diameter (mm). (d) Temporal variations in radar reflectivity (dBZ, blue curve) and rainfall rate (mm h^{-1}, green curve) from 03:55 to 09:00 IST. In panel (a), C, M, and S denote convective, mixed, and stratiform cloud types, respectively.

The simultaneous observations obtained from the ground-based PARSIVEL disdrometer (PSD) and Micro Rain Radar (MRR) over Kadapa on 22 October 2022 reveal distinct temporal variations in radar reflectivity and rain rate. As shown in Figure 4(a), both instruments capture a rapid increase in reflectivity at approximately 1.2 h IST, followed by considerable fluctuations during the initial precipitation phase. A pronounced enhancement occurs between approximately 4.4 and 6.5 h, when reflectivity reaches approximately 25–30 dBZ, indicating the principal precipitation period. The corresponding rain-rate observations in Figure 4(b) exhibit a similar temporal evolution, with the PSD recording maximum values approaching 2.5 mm h^{-1}, while the MRR records peaks of approximately 2.0–2.2 mm h^{-1}. The higher short-duration rain-rate peaks recorded by the PSD suggest differences in the precipitation characteristics sampled by the two instruments. Following the principal rainfall phase, both reflectivity and rain rate decrease considerably after approximately 6.5 h, with intermittent weak precipitation signals persisting until around 11.5 h. The close temporal correspondence between the measurements demonstrates the capability of the two instruments to capture the major stages of precipitation development and dissipation. However, differences in measurement magnitude highlight the importance of considering instrument sampling characteristics and the vertical variability of precipitation when comparing near-surface disdrometer observations with radar-derived measurements [7]–[10], [13], [14].

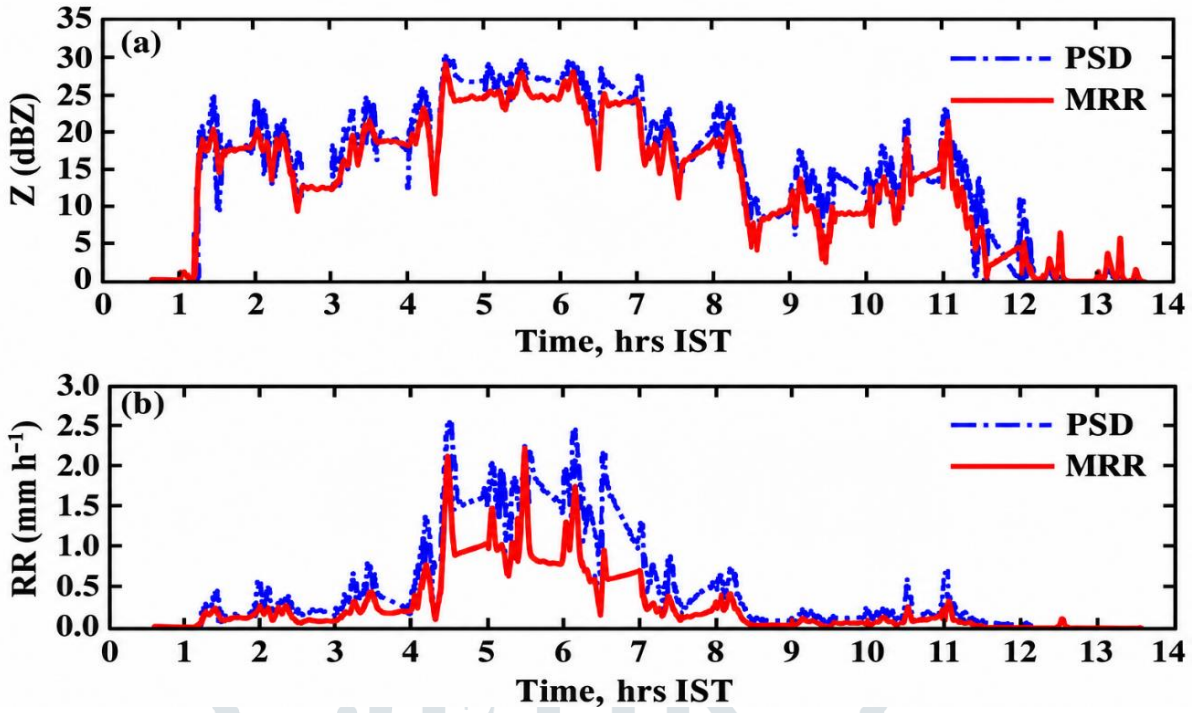

Figure 4 Simultaneous time-series comparison of precipitation measurements obtained from the ground-based PARSIVEL disdrometer and the Micro Rain Radar (MRR) at 300 m above mean sea level (MSL) over Kadapa, Andhra Pradesh, on 22 October 2020. (a) Temporal variation in radar reflectivity (dBZ) and (b) corresponding rain-rate variation (mm h^{-1}), as measured by the PARSIVEL disdrometer (PSD) and MRR. The comparison illustrates the temporal agreement and differences between near-surface and elevated radar-derived precipitation measurements during the rainfall event

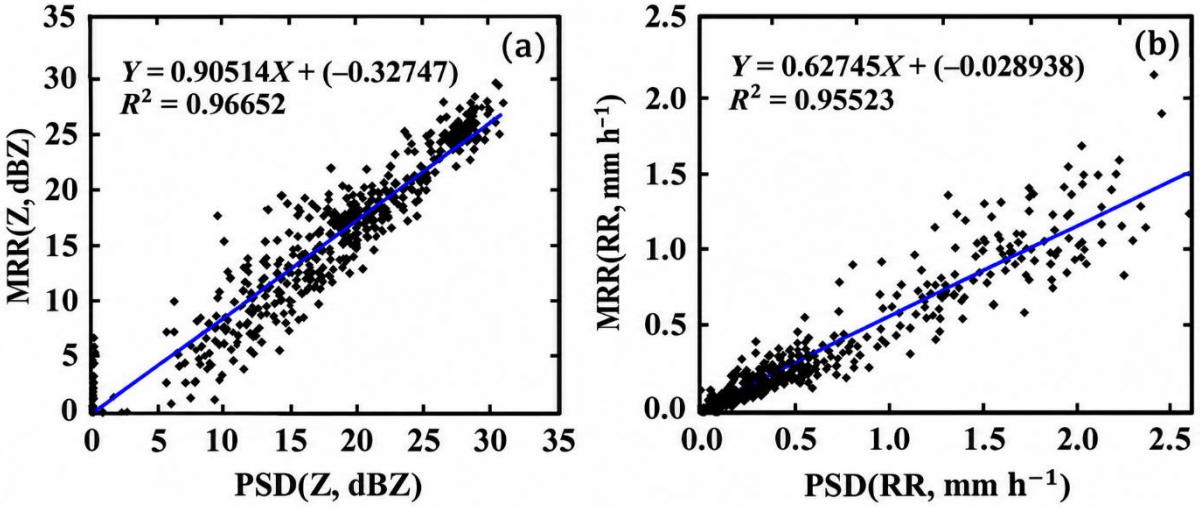

Figure 5. Scatter-plot comparison of simultaneous measurements obtained from the PARSIVEL disdrometer (PSD) and Micro Rain Radar (MRR): (a) radar reflectivity (Z, dBZ) and (b) rain rate (RR, mm h^{-1}). The scatter distributions, linear regression fits, and coefficients of determination (R^2) illustrate the degree of agreement between the two measurement systems.

The scatter-plot comparison of radar reflectivity and rain-rate measurements obtained from the PARSIVEL disdrometer (PSD) and Micro Rain Radar (MRR) demonstrates a strong linear association between the two measurement systems. As shown in Figure 5(a), radar reflectivity exhibits a regression relationship of ZMRR=0.90514 ZPSD -0.32747, with a coefficient of determination (R2) of 0.96652. The regression slope, being relatively close to unity, indicates good correspondence between the reflectivity measurements, although a small systematic difference is evident. Similarly, the rain-rate comparison in Figure 5(b) yields a regression equation of RRMRR=0.62745RRPSD - 0.028938, with an (R2) value of 0.95523, indicating a strong linear relationship. However, the considerably lower regression slope suggests that MRR-derived rain rates are generally lower than the corresponding PSD measurements, with the difference becoming more apparent at higher rain rates. The relatively greater dispersion of data points in the rain-rate comparison also indicates increased variability between the instruments under more intense precipitation conditions. These differences may be attributed to their distinct measurement principles, sampling volumes, temporal resolution, and sensitivity to raindrop-size distributions. Overall, the results demonstrate strong statistical correspondence between PSD and MRR measurements, particularly for radar reflectivity, while highlighting the need to account for systematic differences when comparing rain-rate estimates [7]–[10], [13]–[15].

The integrated ground-based observational network provides a valuable framework for investigating thunderstorms and precipitation microphysics over Kadapa. Nevertheless, agreement between two instruments does not necessarily establish their absolute accuracy. In particular, the strong statistical relationship between MRR and PARSIVEL observations should be interpreted as evidence of measurement consistency rather than proof of calibration accuracy [8]–[10], [13], [14].

4.2 Ground-based Lightning Sensor validation using Satellite observations

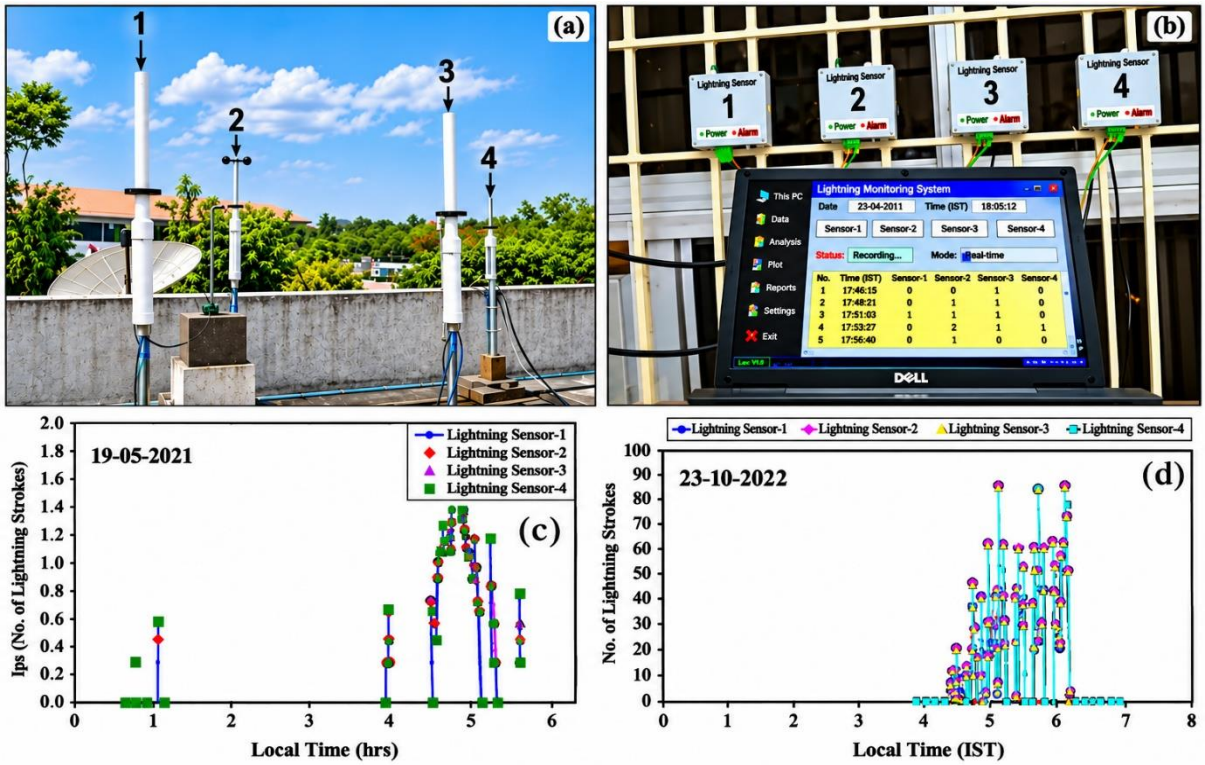

Figure 6. Field deployment of Lightning Senor monitoring system, and temporal distribution of lightning activity recorded by a four-sensor lightning detection network. (a) Outdoor installation of four lightning sensors (1–4) at the observation site; (b) indoor lightning monitoring system showing the four sensor units connected to the data acquisition and monitoring interface; (c) temporal variation in lightning strokes recorded by Lightning Sensors 1–4 on 19 May 2021, expressed as strokes per second (IPS) against local time (IST); and (d) temporal distribution of the number of lightning strokes detected by the four sensors on 23 October 2022. The observations demonstrate the temporal characteristics and sensor-wise variations in detected lightning activity during the two observation periods..

In addition to the long-term climatological observations, high-resolution lightning telemetry was examined for selected thunderstorm events during October 2021 and 2022. Particular attention was given to the lightning activity recorded during the 11–16 October 2022 observation interval, including the lightning distribution presented for 16 October 2022. The event-based dataset comprises lightning stroke counts, temporal occurrence, event duration and variations in the recorded activity. Measurements from the multiple lightning sensors were used to investigate the temporal evolution of lightning activity and compare the stroke records obtained from individual sensors (as shown in Figure 6). The October 2022 observations provide an event-scale perspective that complements the long-term thunderstorm climatology. Previous satellite-based investigations over Telangana, Rayalaseema and coastal Andhra Pradesh have also demonstrated distinct seasonal variations in lightning activity, with prominent pre-monsoon and post-monsoon maxima [6]–[18], [26]–[28].

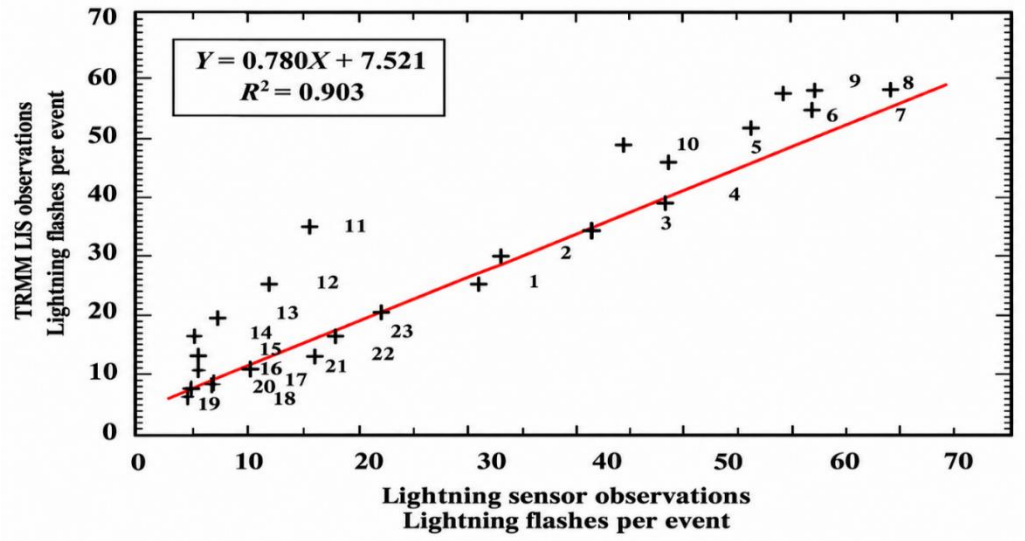

Figure 7. Scatter plot comparing lightning flashes per thunderstorm event recorded by the ground-based lightning sensor and the TRMM Lightning Imaging Sensor (LIS) for 23 thunderstorm cases, illustrating the relationship between the two observational datasets.

This study evaluates the performance of ground-based lightning detection sensors deployed at Kadapa, Andhra Pradesh, by comparing their observations with total lightning measurements obtained from the satellite-based Tropical Rainfall Measuring Mission (TRMM)

Lightning Imaging Sensor (LIS). The analysis considers 23 thunderstorm events recorded during the northeast monsoon seasons (October–December) of 2021 and 2022. Figure 7 illustrates the event-wise relationship between ground-based lightning sensor observations (X-axis) and TRMM-LIS observations (Y-axis), expressed as the number of lightning flashes per event. The scatter plot reveals a strong positive linear association between the two observing systems, indicating that higher lightning flash counts recorded by the ground-based sensors generally correspond to higher counts detected by TRMM-LIS. The approximate linear regression equation is Y = 0.780X + 7.521, with a coefficient of determination (R^2) of 0.903 and a correlation coefficient (r) of approximately 0.950. This indicates that approximately 90.3% of the variability in the TRMM-LIS flash counts is explained by the fitted linear relationship. The observed differences between the two datasets may be attributed to variations in sensor sensitivity, detection thresholds, lightning characteristics, spatial coverage, temporal sampling, and the distinct measurement principles employed by the ground-based and satellite-based systems [6]–[18], [26]–[28].

4.3 GPS Radiosonde Data Quality Assessment and Thermodynamical parameters calculation:

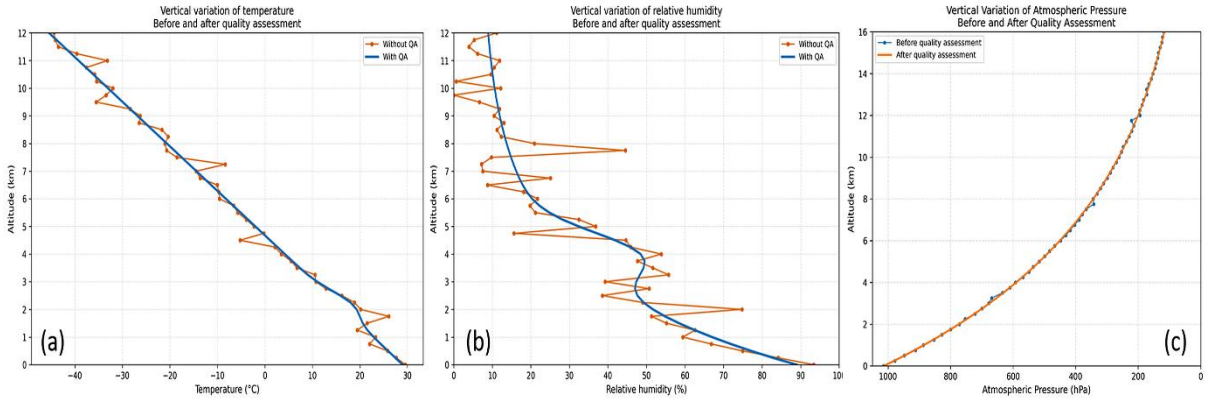

Figure 8: Vertical profiles of (a) environmental temperature, (b) relative humidity, and (c) atmospheric pressure recorded by the GPS radiosonde over Kadapa on 22 August 2021 at 11:30 IST, before and after quality assessment (QA). The comparison highlights the identification and correction of irregular variations in the temperature and relative humidity profiles, while the atmospheric pressure profile exhibits a consistent decrease with increasing altitude. Overall, the QA procedure improves the vertical continuity and physical consistency of the radiosonde observations, providing a more reliable basis for subsequent thermodynamic analysis.

.

Radiosonde observations provide essential information on the vertical thermodynamic structure of the atmosphere and are widely used to assess atmospheric instability and thunderstorm development. A GPS radiosonde, attached to a weather balloon, measures atmospheric pressure, temperature, relative humidity and wind speed and direction at different altitudes during its ascent (as shown2(c)). Figure 8 compares the vertical profiles of temperature, relative humidity, and atmospheric pressure recorded by the GPS radiosonde on 22 August 2021 at 11:30 IST, before and after quality assessment (QA). Figure 8(a) shows that the temperature profile exhibits several irregular fluctuations and isolated deviations before QA. Following QA, the profile becomes smoother and more vertically consistent while retaining the overall decrease in temperature with increasing altitude. Figure 8(b) illustrates the vertical variation of relative humidity. The unprocessed profile exhibits considerable fluctuations, including abrupt variations at different altitudes. After QA, these irregularities are reduced, resulting in a more continuous profile and a clearer representation of the vertical moisture distribution. Figure 8(c) presents the atmospheric pressure profiles before and after QA. Both profiles show a consistent decrease in pressure with increasing altitude. Their close agreement indicates that the pressure measurements undergo comparatively little change during the QA procedure [19]–[25].
Overall, the comparison demonstrates that QA primarily improves the vertical continuity and physical consistency of the temperature and relative humidity profiles, whereas the atmospheric pressure profile remains nearly unchanged. These quality-controlled radiosonde observations provide a more reliable basis for calculating atmospheric stability parameters, including Convective Available Potential Energy (CAPE), Convective Inhibition (CIN), and other thermodynamic indices relevant to thunderstorm analysis.

A radiosonde sounding provides vertical profiles of pressure (p), air temperature (T), dew-point temperature (Td), and wind direction (D) and speed (V). The indices below are calculated from thermodynamic values at standard pressure levels and, for Available Potential Energy (CAPE), Convective Inhibition (CIN), from the full vertical profile. Temperatures used in lapse-rate and index equations are conventionally expressed in °C; thermodynamic calculations involving gas laws and virtual temperature require kelvin [19]–[23].

Variable	Required level/profile	Use
T and Td	850, 700 and 500 hPa	TTI and K-index
D and V	850 and 500 hPa	SWEAT index
p, T and Td	Complete sounding profile	Parcel path, CAPE and CIN
Surface pressure and surface T/Td	Surface parcel definition	Surface-based CAPE/CIN

The following table provides the equations and calculation methods for 1. Convective Available Potential Energy (CAPE); 2.Convective Inhibition (CIN), 3.Total Totals Index (TTI), 4.K-Index (KI/KX), and 5.Severe Weather Threat (SWEAT) Index [20]–[23]

Parameter	Equation / basis	Radiosonde inputs	Unit
CAPE	$\int$LFC→EL g[(Tv,p−Tv,e)/Tv,e] dz	Full p–T–Td profile; parcel definition	J kg^{-1}
CIN	$-\int$ origin→LFC g[(Tv,p−Tv,e)/Tv,e] dz over negative buoyancy	Full p–T–Td profile; parcel definition	J kg^{-1}
TTI	T850 + Td850 − 2T500	T850, Td850, T500	°C / index
KI/KX	(T850−T500)+Td850−(T700−Td700)	T850, Td850, T700, Td700, T500	°C / index
SWEAT	12Td850 + 20(TTI−49) + 2V850 + V500 + 125[sin(ΔD)+0.2], with gates	Td850, TTI, D/V at 850 and 500 hPa	Dimensionless

Higher CAPE values generally indicate greater potential for vigorous convection, although thunderstorm intensity also depends on moisture availability, vertical wind shear, convective inhibition and other atmospheric conditions. Therefore, radiosonde-derived CAPE provides an important thermodynamic parameter for investigating atmospheric instability and assessing the potential for thunderstorm development over the Kadapa region [19]–[23].

The GPS radiosonde sounding over Kadapa indicates a potentially favourable environment for deep convective development, characterized by substantial CAPE (2,200 J kg^{-1}), a CIN magnitude of approximately 110 J kg^{-1} and appreciable lower-tropospheric moisture. The vertical separation between temperature and dew-point profiles suggests variations in atmospheric moisture with height, which may influence cloud development, precipitation processes and downdraft characteristics. These thermodynamic conditions provide a plausible atmospheric background for thunderstorm occurrence over the study region [19]–[21], [24].

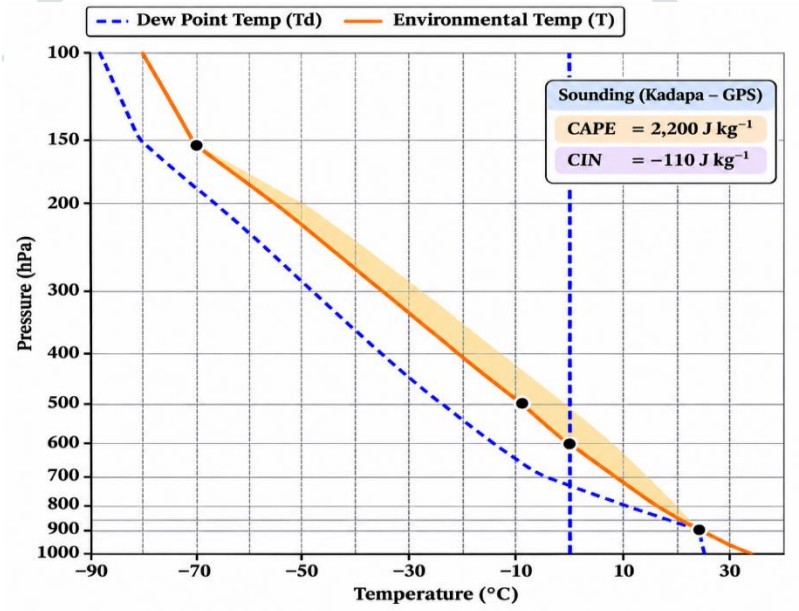

Figure 9. Typical thermodynamic structure of a thunderstorm event over Kadapa, derived from GPS radiosonde observations. The temperature and dew-point profiles indicate moist conditions in the lower troposphere, a pronounced separation between the profiles in the mid-troposphere, and steep environmental temperature gradients. These features suggest an environment favourable for convective development, with potentially high Convective Available Potential Energy (CAPE), relatively low Convective Inhibition (CIN), and enhanced downdraft potential

V. RESULTS AND DISCUSSIONS:

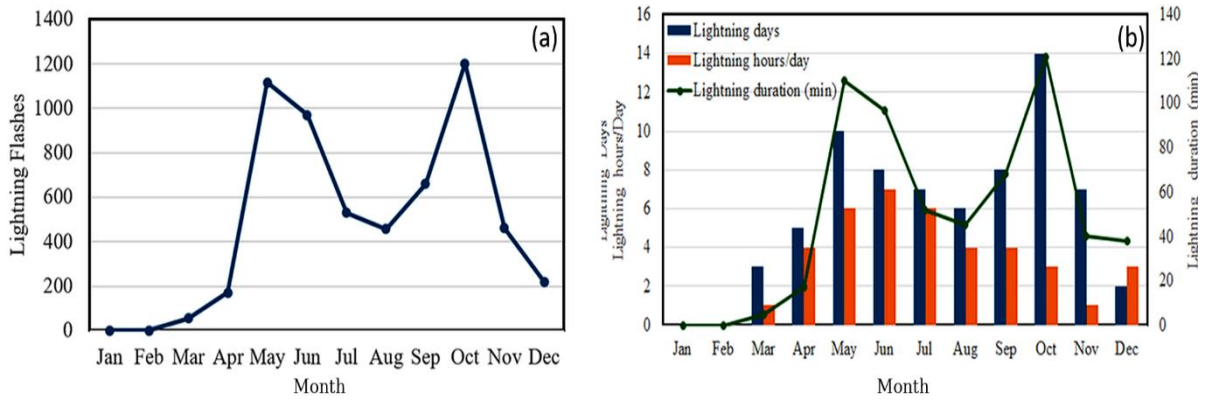

Figure 10. Monthly variation in lightning activity over Kadapa. (a) Monthly distribution of lightning flashes recorded by the ground-based lightning detection system. (b) Monthly variations in the number of lightning days, average lightning hours per day, and lightning duration (min). The observations illustrate the seasonal distribution and temporal characteristics of lightning activity.

The figure illustrates the monthly and seasonal variability of lightning activity over Kadapa. As shown in Figure 10(a), lightning flashes exhibit a distinct bimodal pattern, with prominent peaks during May (approximately 1,110 flashes) and October (approximately

1,200 flashes). Activity increases gradually from March, reaches its first maximum in May, and decreases during July and August before rising again in September and October. A subsequent decline is observed during November and December [1]–[3], [16], [17]. Figure 10(b) shows corresponding variations in lightning days, average lightning hours per day, and lightning duration. October records the highest number of lightning days (approximately 14 days) and the longest lightning duration (approximately 120 min). May also exhibits substantial activity, with approximately 10 lightning days and a lightning duration of about 110 min. In contrast, the average lightning hours per day reach their highest value in June (approximately 7 hours), indicating that the monthly maximum in daily lightning activity does not necessarily coincide with the maximum number of lightning days or total lightning duration.
Overall, the observations indicate two prominent periods of enhanced lightning activity over Kadapa: the pre-monsoon period (April–May) and the post-monsoon period (September–October). The pronounced October maximum suggests enhanced lightning occurrence during the post-monsoon season, while the May peak highlights significant pre-monsoon convective activity [1]–[3], [16], [17].

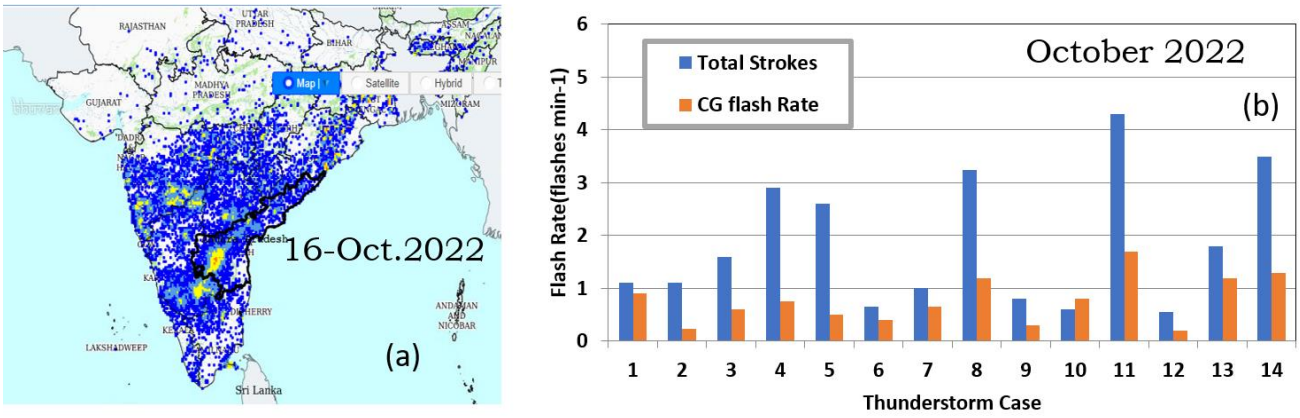

Figure 11 Spatial distribution and case-wise characteristics of lightning activity over India during October 2022. (a) Spatial distribution of detected lightning events over southern India on 16 October 2022, showing the geographical extent and regional concentration of lightning activity. (b) Total lightning stroke rate (blue bars) and cloud-to-ground (CG) flash rate (orange bars) recorded during 14 thunderstorm cases in October 2022. The comparison illustrates variations in total lightning activity and CG flash rates among the observed thunderstorm events.

The spatial distribution in Figure 11(a) indicates widespread lightning activity over southern India on 16 October 2022, with a particularly dense concentration of detected events over the central and southern parts of the study region. The distribution also suggests considerable spatial variability, indicating that lightning activity was not uniformly distributed across the region [6]–[18], [26]–[28].
Figure 11(b) demonstrates substantial case-to-case variability in lightning activity during the 14 thunderstorm events. Total lightning stroke rates were generally higher than CG flash rates, indicating that cloud-to-cloud and intracloud discharges contributed considerably to the overall lightning activity. The highest total stroke rate occurred during Case 11, reaching approximately 4.3 flashes min^{-1}, accompanied by a CG flash rate of approximately 1.7 flashes min^{-1}. Relatively high total stroke rates were also observed during Cases 14, 8 and 4. In contrast, Cases 6, 9, 10 and 12 exhibited comparatively lower total lightning activity [5], [6], [26], [27].
The differences between total lightning and CG flash rates highlight the importance of considering both total lightning activity and CG discharges when characterizing thunderstorm electrical behaviour. In particular, total lightning measurements provide a broader representation of electrical activity within convective clouds than CG observations alone. The figure supports comparisons of lightning activity among the 14 cases, but it does not by itself establish relationships with rainfall intensity, storm severity or cloud microphysical processes. Those interpretations would require additional meteorological observations.

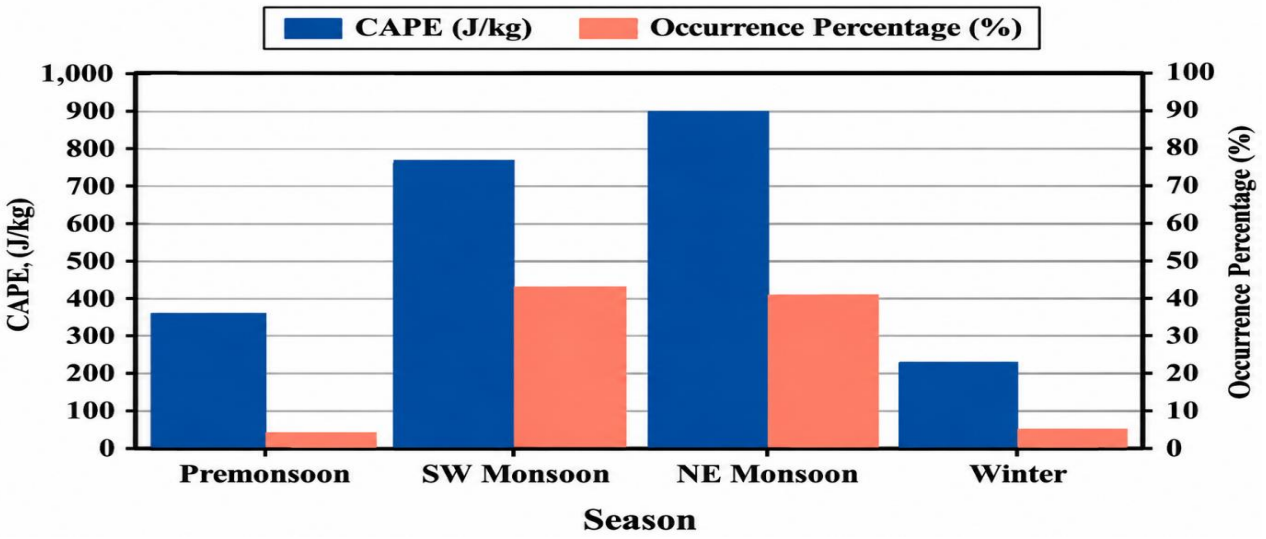

Figure 12. Seasonal variation in convective available potential energy (CAPE, J kg^{-1}) and thunderstorm occurrence percentage (%) across the pre-monsoon, southwest monsoon, northeast monsoon, and winter seasons. Blue bars represent CAPE, while coral bars indicate thunderstorm occurrence percentage.

Figure 12 illustrates the seasonal variation in convective available potential energy (CAPE) and thunderstorm occurrence over the study region. The northeast monsoon exhibits the highest CAPE (900, scaled value), followed by the southwest monsoon (769), pre-monsoon (360), and winter (229). In contrast, thunderstorm occurrence is highest during the southwest monsoon (45%), followed by the northeast monsoon (41%), pre-monsoon (8%), and winter (6%). The results indicate that although CAPE is highest during the northeast monsoon, thunderstorm occurrence is slightly greater during the southwest monsoon. This suggests that thunderstorm frequency is not governed by atmospheric instability alone; moisture availability, vertical wind shear, and lifting mechanisms may also influence seasonal convective activity [19]–[23].

Overall, the results indicate that thunderstorm activity is concentrated during the southwest and northeast monsoon seasons, accounting for 86% of the total seasonal occurrence. Although higher CAPE generally indicates greater potential for deep convection, the difference between the CAPE maximum and thunderstorm-occurrence maximum suggests that atmospheric instability alone does not determine thunderstorm frequency. Moisture availability, vertical wind shear, lifting mechanisms, and regional atmospheric circulation may also influence seasonal thunderstorm development [1]–[4], [19]–[23].

5.3 Integrated Framework for Multi-Instrument Thunderstorm and Precipitation Classification

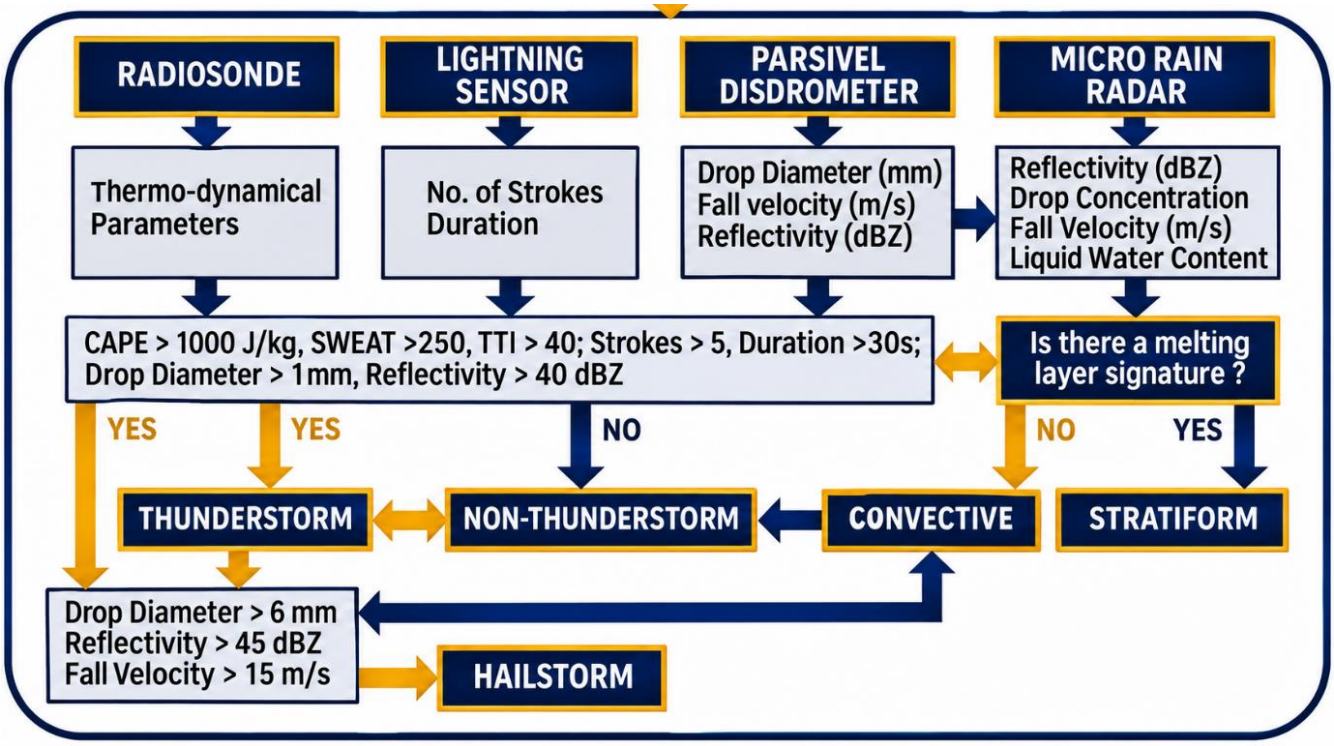

Figure 13. Flowchart illustrating the integrated multi-instrument methodology for thunderstorm, non-thunderstorm, convective, stratiform, and hailstorm classification using radiosonde-derived thermodynamic parameters, lightning sensor observations, PARSIVEL disdrometer measurements, and Micro Rain Radar (MRR) observations. The classification framework applies predefined thresholds of CAPE, SWEAT, TTI, lightning stroke count and duration, raindrop diameter, reflectivity, and fall velocity, together with melting-layer signature detection, to distinguish precipitation and storm types.

Figure 13 presents an integrated multi-instrument approach to classifying thunderstorms and precipitation systems over Kadapa. Radiosonde data provide atmospheric instability indices (CAPE, SWEAT and TTI), lightning sensors measure stroke count and duration, PARSIVEL provides raindrop size and fall velocity, and MRR measures reflectivity and vertical precipitation characteristics. Applying predefined thresholds, the framework distinguishes thunderstorm and non-thunderstorm events, further classifies precipitation into convective and stratiform types using melting-layer signatures, and identifies potential hailstorm conditions based on hydrometeor diameter, reflectivity and fall velocity. This integrated approach combines atmospheric, electrical and microphysical observations for comprehensive storm classification [7]–[15], [20]–[25].

The distribution indicates considerable day-to-day and hour-to-hour variability in precipitation-system occurrence. The classified events are irregularly distributed throughout the observation period rather than occurring continuously. Several precipitation-system categories appear at different times of the day, suggesting that the observed precipitation activity involves diverse atmospheric processes and varying convective conditions [11], [12], [29].

Convective and mixed precipitation classifications are observed across several Julian Days, particularly around Days 109–123 and 129–135. The presence of these categories indicates the occurrence of precipitation systems involving convective processes, either independently or in combination with other precipitation structures. Their temporal distribution suggests intermittent

The occurrence of classifications involving TS and HS indicates that some precipitation events were associated with thunderstorm and hailstorm conditions. These classifications appear intermittently, with notable concentrations around Julian Days 121–123, 133–135 and 143–148. This distribution suggests that thunderstorm-related precipitation systems were not uniformly distributed throughout the observation period.

The presence of mixed and stratiform-related classifications, including M/NTS and S/NT, indicates that precipitation activity also occurred under non-thunderstorm conditions. These categories appear at multiple Julian Days and hourly intervals, demonstrating the diversity of precipitation regimes. Their occurrence alongside convective classifications suggests that the study period captured both convective and comparatively organized or non-thunderstorm precipitation structures.

The hourly distribution shows that precipitation-system classifications occurred during both daytime and nighttime periods. Several events are observed during the early hours, while others appear during afternoon and evening intervals. This indicates that precipitation occurrence was not restricted to a particular time of day. However, the figure alone does not establish a statistically significant diurnal preference because the total number

The temporal distribution demonstrates substantial variability in precipitation-system classifications over Julian Days 107–149. The simultaneous occurrence of convective, mixed and stratiform precipitation categories, together with thunderstorm-, hailstorm- and non-thunderstorm-associated classifications, highlights the diversity of atmospheric conditions influencing precipitation development over the study region. The intermittent appearance of thunderstorm-related categories suggests episodic convective activity, while the presence of non-thunderstorm classifications indicates that precipitation was also generated under comparatively less electrically active conditions. These results emphasize the importance of considering precipitation type, storm characteristics and hourly variability when investigating the evolution of regional precipitation systems [11], [12], [29].

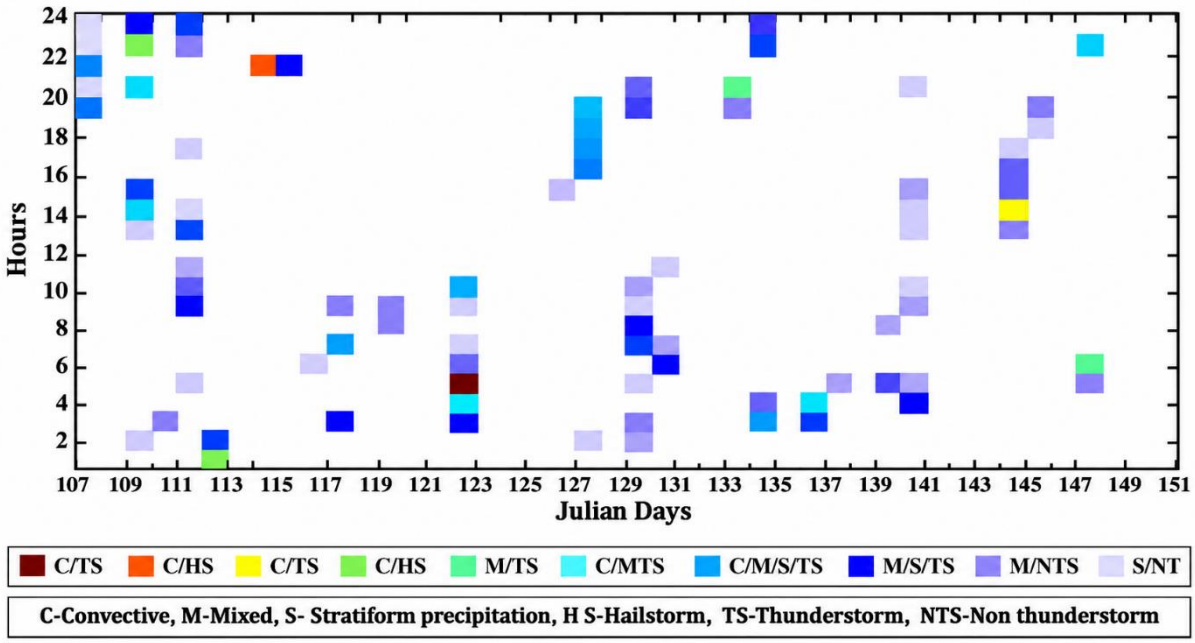

Figure 14. Temporal distribution of precipitation-system classifications over Julian Days 107–149, showing the occurrence of different precipitation types across hourly intervals (approximately 1–24 h). The coloured squares represent combinations of convective (C), mixed (M), and stratiform (S) precipitation associated with hailstorms (HS), thunderstorms (TS), and non-thunderstorms (NTS), illustrating the temporal variability and diversity of precipitation regimes during the observation period.

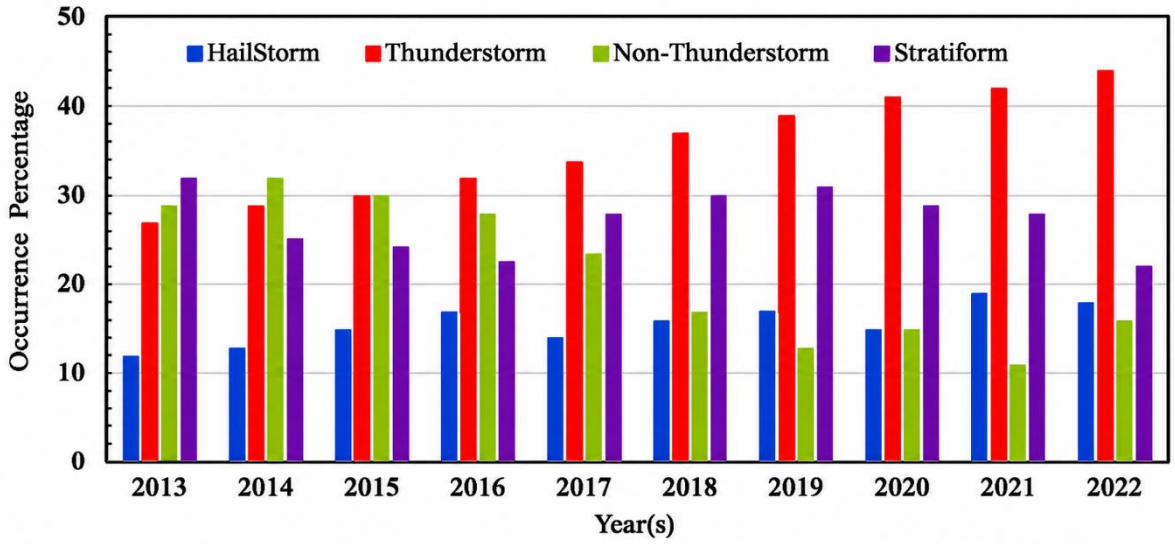

Figure 15. Year-wise variation in the occurrence percentage of hailstorms and thunderstorms over the period 2013–2022. The grouped bar chart illustrates interannual variability in storm occurrence, with hailstorm and thunderstorm percentages represented by blue and red bars, respectively. The green and purple bars show two additional plotted categories whose labels are not visible in the legend. The results indicate a general increase in thunderstorm occurrence percentage from 2013 to 2022, while hailstorm occurrence exhibits comparatively smaller year-to-year variations.

Thunderstorms (red bars) exhibit a progressive increase in occurrence percentage over the study period, rising from approximately 27% in 2013 to 44% in 2022. A particularly noticeable increase occurs between 2016 and 2018, followed by a relatively steady rise

through 2022. This pattern indicates an increasing contribution of thunderstorm-associated events to the annual precipitation-system classifications [1]–[3], [16], [17].

Hailstorms (blue bars) exhibit comparatively moderate interannual variability, with occurrence percentages ranging approximately from 12% to 19%. The highest value occurs in 2021, followed by a slight decrease in 2022. Unlike thunderstorms, hailstorms do not demonstrate a consistent increasing or decreasing trend throughout the observation period.

Non-thunderstorm events (green bars) show a notable declining tendency, decreasing from approximately 32% in 2014 to around 11% in 2021, before increasing slightly to approximately 16% in 2022. This reduction suggests a decreasing relative contribution of non-thunderstorm precipitation classifications during the later years of the study period.

Stratiform precipitation (purple bars) exhibits moderate fluctuations, with occurrence percentages ranging from approximately 22% to 32%. Higher values are observed during 2013 and 2019, whereas comparatively lower values occur during 2016 and 2022. The overall pattern suggests variability rather than a consistent long-term increase or decrease.

The interannual distribution demonstrates a contrasting behaviour among the four precipitation-system categories. Thunderstorm occurrence shows a clear upward tendency, increasing from approximately 27% in 2013 to 44% in 2022, while non-thunderstorm occurrence generally decreases. Hailstorm occurrence remains comparatively stable, despite moderate year-to-year fluctuations, and stratiform precipitation exhibits intermittent variations throughout the study period.

These contrasting patterns indicate changes in the relative composition of precipitation-system classifications over the observation period, with an increasing proportion of thunderstorm-associated events and a declining contribution from non-thunderstorm events. The results emphasize the importance of examining long-term variability in convective and non-convective precipitation systems to understand changes in regional atmospheric behaviour [1]–[3], [16], [17].

VI. CONCLUSIONS:

The integration of these complementary observational systems enables a comprehensive investigation of thunderstorm processes by linking near-surface meteorological conditions, cloud and precipitation microphysics, vertical atmospheric structure, lightning activity and thermodynamic instability within a unified observational framework. The main scientific contribution of this research is the development and application of an integrated, multi-instrument observational framework to characterize thunderstorms over Kadapa, southern India, by examining their electrical activity, atmospheric thermodynamic conditions and precipitation microphysics together [7]–[15], [24], [25].

Rather than analysing lightning, radar rainfall or atmospheric instability independently, the study brings together ground-based lightning sensors, MRR, PARSIVEL disdrometer, GPS radiosonde, automatic weather station and satellite observations to provide complementary evidence of thunderstorm characteristics.

Three key scientific contributions

1. Integrated characterization of thunderstorms: Combines lightning measurements, vertical precipitation profiles, raindrop-size distributions and radiosonde-derived instability parameters to examine different aspects of convective systems.
2. Observational comparison and validation: Demonstrates strong statistical correspondence between MRR and PARSIVEL measurements (reflectivity \(R^2=0.9665\); rainfall rate \(R^2=0.9552\)) and between ground-based lightning observations and TRMM-LIS measurements (\(R^2=0.903\)).
3. Regional characterization and classification: Documents the 2013–2022 lightning variability over Kadapa and presents an integrated framework for distinguishing thunderstorm, non-thunderstorm, hailstorm, convective and stratiform precipitation characteristics using multiple observational parameters.

The principal scientific contribution of this study is the integration of multi-instrument atmospheric observations to characterize the electrical, thermodynamic and microphysical properties of thunderstorms over Kadapa, southern India. By combining long-term lightning records, satellite observations, MRR-derived vertical precipitation profiles, PARSIVEL raindrop-size distributions and radiosonde-derived instability parameters, the study provides a complementary observational perspective on regional convective activity. The inter-instrument comparisons establish strong statistical correspondence between precipitation and lightning measurements, while the integrated classification framework provides a basis for distinguishing different thunderstorm and precipitation regimes. These findings contribute to the regional understanding of thunderstorm variability and demonstrate the value of coordinated ground-based and satellite observations for investigating convective precipitation systems.

ACKNOWLEDGMENT

The authors thank the Coordinator, Semi-Arid Zonal Atmospheric Research Centre (SARC), Department of Physics, Yogi Vemana University, Kadapa, for the facilities and support provided during this work. The authors also acknowledge the authorities of Yogi Vemana University, Kadapa, for their encouragement and administrative sanctions that enabled this research.

REFERENCES

[1] G. K. Manohar and A. P. Kesarkar, “Climatology of thunderstorm activity over the Indian region: A study of east–west contrast,” MAUSAM, vol. 54, no. 4, pp. 819–828, Oct. 2003, doi: 10.54302/mausam.v54i4.1581.

[2] G. K. Manohar and A. P. Kesarkar, “Climatology of thunderstorm activity over the Indian region: II. Spatial distribution,” MAUSAM, vol. 55, no. 1, pp. 31–40, Jan. 2004, doi: 10.54302/mausam.v55i1.854.

[3] G. K. Manohar and A. P. Kesarkar, “Climatology of thunderstorm activity over the Indian region: III. Latitudinal and seasonal variation,” MAUSAM, vol. 56, no. 3, 2005, doi: 10.54302/mausam.v56i3.987.

[4] R. A. Houze Jr., “Stratiform precipitation in regions of convection: A meteorological paradox?,” Bull. Amer. Meteor. Soc., vol. 78, no. 10, pp. 2179–2196, Oct. 1997, doi: 10.1175/1520-0477(1997)078<2179:SPIROC>2.0.CO;2.

[5] C. P. R. Saunders, “Charge separation mechanisms in clouds,” Space Sci. Rev., vol. 137, pp. 335–353, 2008, doi: 10.1007/s11214-008-9345-0.

[6] H. J. Christian et al., "Global frequency and distribution of lightning as observed from space by the Optical Transient Detector," J. Geophys. Res.: Atmos., vol. 108, no. D1, Art. no. 4005, 2003, doi: 10.1029/2002JD002347.
[7] G. Peters, B. Fischer, and T. Andersson, "Rain observations with a vertically looking Micro Rain Radar (MRR)," Boreal Environ. Res., vol. 7, pp. 353–362, 2002.
[8] M. Löffler-Mang, M. Kunz, and W. Schmid, "On the performance of a low-cost K-band Doppler radar for quantitative rain measurements," J. Atmos. Oceanic Technol., vol. 16, no. 3, pp. 379–387, Mar. 1999, doi: 10.1175/1520-0426(1999)016<0379:OTPOAL>2.0.CO;2.
[9] A. Tokay, D. B. Wolff, and W. A. Petersen, "Evaluation of the new version of the laser-optical disdrometer, OTT Parsivel2," J. Atmos. Oceanic Technol., vol. 31, no. 6, pp. 1276–1288, Jun. 2014, doi: 10.1175/JTECH-D-13-00174.1.
[10] M. Maahn and P. Kollias, "Improved Micro Rain Radar snow measurements using Doppler spectra post-processing," Atmos. Meas. Tech., vol. 5, no. 11, pp. 2661–2673, Nov. 2012, doi: 10.5194/amt-5-2661-2012.
[11] M. Steiner, R. A. Houze Jr., and S. E. Yuter, "Climatological characterization of three-dimensional storm structure from operational radar and rain gauge data," J. Appl. Meteorol., vol. 34, no. 9, pp. 1978–2007, Sep. 1995, doi: 10.1175/1520-0450(1995)034<1978:CCOTDS>2.0.CO;2.
[12] D. Atlas, R. C. Srivastava, and R. S. Sekhon, "Doppler radar characteristics of precipitation at vertical incidence," Rev. Geophys., vol. 11, no. 1, pp. 1–35, Feb. 1973, doi: 10.1029/RG011i001p00001.
[13] C. W. Ulbrich, "Natural variations in the analytical form of the raindrop size distribution," J. Climate Appl. Meteorol., vol. 22, no. 10, pp. 1764–1775, Oct. 1983, doi: 10.1175/1520-0450(1983)022<1764:NVITAF>2.0.CO;2.
[14] V. N. Bringi and V. Chandrasekar, Polarimetric Doppler Weather Radar: Principles and Applications. Cambridge, U.K.: Cambridge Univ. Press, 2001, doi: 10.1017/CBO9780511541094.
[15] L. Baldini et al., "Rainfall and DSD parameters comparison between Micro Rain Radar, two-dimensional video and Parsivel2 disdrometers, and S-band dual-polarization radar," J. Atmos. Oceanic Technol., vol. 37, no. 4, pp. 621–640, Apr. 2020, doi: 10.1175/JTECH-D-19-0085.1.
[16] D. J. Cecil, D. E. Buechler, and R. J. Blakeslee, "Gridded lightning climatology from TRMM-LIS and OTD: Dataset description," Atmos. Res., vols. 135–136, pp. 404–414, 2014, doi: 10.1016/j.atmosres.2012.06.028.
[17] D. J. Cecil, D. E. Buechler, and R. J. Blakeslee, "TRMM LIS climatology of thunderstorm occurrence and conditional lightning flash rates," J. Climate, vol. 28, no. 16, pp. 6536–6547, 2015, doi: 10.1175/JCLI-D-15-0124.1.
[18] C. Kummerow et al., "The Tropical Rainfall Measuring Mission (TRMM) sensor package," J. Atmos. Oceanic Technol., vol. 15, no. 3, pp. 809–817, Jun. 1998, doi: 10.1175/1520-0426(1998)015<0809:TTRMTS>2.0.CO;2.
[19] C. A. Doswell III and E. N. Rasmussen, "The effect of neglecting the virtual temperature correction on CAPE calculations," Weather Forecasting, vol. 9, no. 4, pp. 625–629, Dec. 1994, doi: 10.1175/1520-0434(1994)009<0625:TEONTV>2.0.CO;2.
[20] E. N. Rasmussen and D. O. Blanchard, "A baseline climatology of sounding-derived supercell and tornado forecast parameters," Weather Forecasting, vol. 13, no. 4, pp. 1148–1164, Dec. 1998, doi: 10.1175/1520-0434(1998)013<1148:ABCOSD>2.0.CO;2.
[21] J. M. Craven and H. E. Brooks, "Baseline climatology of sounding-derived parameters associated with deep, moist convection," Natl. Wea. Dig., vol. 28, no. 1, pp. 13–24, 2004.
[22] R. C. Miller, Notes on Analysis and Severe-Storm Forecasting Procedures of the Air Force Global Weather Central. Air Weather Service Technical Report 200 (Rev.), 1972.
[23] J. J. George, Weather Forecasting for Aeronautics. New York, NY, USA: Academic Press, 1960.
[24] World Meteorological Organization, Guide to Instruments and Methods of Observation, WMO-No. 8, Geneva, Switzerland, 2018 ed.
[25] World Meteorological Organization, Manual on the Global Observing System, WMO-No. 544, Geneva, Switzerland, 2015 ed.
[26] D. J. Boccippio et al., "The Optical Transient Detector (OTD): Instrument characteristics and cross-sensor validation," J. Atmos. Oceanic Technol., vol. 17, no. 4, pp. 441–458, Apr. 2000.
[27] V. A. Rakov and M. A. Uman, Lightning: Physics and Effects. Cambridge, U.K.: Cambridge Univ. Press, 2003.
[28] H. R. Pruppacher and J. D. Klett, Microphysics of Clouds and Precipitation, 2nd rev. and enl. ed. Dordrecht, The Netherlands: Kluwer Academic Publishers, 1997.
[29] R. A. Houze Jr., Cloud Dynamics, 2nd ed. Amsterdam, The Netherlands: Academic Press, 2014.
[30] D. R. MacGorman and W. D. Rust, The Electrical Nature of Storms. ISBN: 9780195073379, New York, NY, USA: Oxford Univ. Press, 1998.